

Structure and vibrational assignment of bis(4-amino-3-penten-2-onato)nickel(II). A density functional theoretical study

M. Jamialahmadi^a, S.F. Tayyari^{b,*}, M.H. Habibi^c, M. Yazdanbakhsh^a, R.E. Sammelson^d

^a Chemistry Department, Ferdowsi University of Mashhad, Mashhad 91775-1436, Iran

^b Department of Chemistry, Neyshabur Branch, Islamic Azad University, Neyshabur, Iran

^c Department of Chemistry, University of Isfahan, Isfahan 81746-73441, Iran

^d Department of Chemistry, Ball State University, Muncie, IN 47306-0445, USA

ARTICLE INFO

Article history:

Received 27 January 2011

Received in revised form 4 May 2011

Accepted 5 May 2011

Available online 11 May 2011

Keywords:

Bis(4-amino-3-penten-2-onato)nickel(II)

FT-IR spectroscopy

FT-Raman spectroscopy

Vibrational assignment

Density functional theory

ABSTRACT

Bis(4-amino-3-penten-2-onato) nickel(II), (Ni(APO)₂), and its NH deuterated analog, Ni(DAPO)₂, were synthesized and their molecular structure and vibrational assignments were investigated by means of density functional theory (DFT) calculations. The molecular stability was investigated by applying the NBO and geometry calculations. The harmonic vibrational frequencies of Ni(APO)₂ and Ni(DAPO)₂ were obtained at the B3LYP level using 6-311G* basis set. The calculated geometrical parameters and vibrational frequencies were compared with the experimental results. The measured vibrational band frequencies were interpreted in terms of the calculated vibrational normal modes. The scaled theoretical frequencies and the structural parameters were found to be in good agreement with the experimental data.

© 2011 Elsevier B.V. All rights reserved.

1. Introduction

In recent years, the use of amine and imine complexes based on late transition metals as active and selective catalysts for the polymerization of α -olefins has received a great deal of attention [1–7]. The late transition metal complexes, because of their less oxophilic nature relative to early transition metal complexes, are generally considered to be more tolerant toward polar media and polar functional groups and thus make them possible targets for the development of catalysts for polar monomer polymerizations [5,8].

Ni is known to be an excellent catalyst for many processes. He and Wu [9] synthesized and characterized a series of bis(β -ketoamino)nickel(II) complexes and investigated the effects of catalyst structure and polymerization conditions on the polymerization activity of methyl methacrylate using bis(β -ketoamino)nickel(II)/methylaluminoxane (MAO) as catalytic systems [10].

According to Gurr's study [11], the unit cell of bis(4-amino-3-penten-2-onato) nickel(II) [hereafter abbreviated as Ni(APO)₂], is orthorhombic, space group Ccca, and the unit cell dimensions are $a = 16.7$, $b = 15.1$, $c = 13.5$ Å. In this research, the complex was prepared in high purity and experimental data were compared with the theoretical calculation results.

2. Experimental

The APO ligand was synthesized according to Lacey [12]. This ligand was added to an aqueous solution of nickel (II) acetate and Ni(APO)₂ was obtained as a precipitate. This precipitate was purified by crystallization from a chloroform solution. Anal. Found: C, 47.52; H, 6.42; N, 10.66; Ni, 23.19. Calc.: NiC₁₀H₁₆O₂N₂: C, 47.11; H, 6.33; N, 10.99; Ni, 23.02%. M.p. 245 °C, ¹H NMR (CDCl₃, 100 MHz, reference: solvent residual peak, δ 7.24 ppm): δ 9.66(b, 2H, NH), δ 4.83(s, 2H, CH), δ 1.84(s, 6H, CH₃CO), δ 1.58(s, 6H, CH₃CN).

The NH deuterated analog of Ni(APO)₂, referred to as Ni(DAPO)₂, was prepared according to the literature [13].

The infrared spectra in the region 500–4000 cm⁻¹ were recorded on a Bomem MB-154 Fourier transform spectrophotometer using KBr pellets and CHCl₃ and CH₂Cl₂ solutions. The spectra were collected with a resolution of 2 cm⁻¹ by signal averaging the results of 15 scans.

The Far-IR spectra of CsBr pellets of Ni(APO)₂ in the 600–150 cm⁻¹ region were obtained by using a ThermoNicolet NEXUS 870 FT-IR spectrometer equipped with a DTGS/polyethylene detector and a solid substrate beam splitter. The spectra were collected with a resolution of 2 cm⁻¹ by averaging the results of 64 scans.

The FT-Raman spectra in the region 3200–200 cm⁻¹ were recorded employing a 180° back-scattering geometry and a Bomem MB-154 Fourier transform Raman spectrometer operating

* Corresponding author. Tel.: +98 9153103538.

E-mail address: sftayyari@hotmail.com (S.F. Tayyari).

at the 1064 nm excitation line of a Nd:YAG laser. It was equipped with a ZnSe beam splitter and a TE cooled InGaAs detector. Rayleigh filtration was afforded by a set of two holographic technology filters. The spectra were accumulated for 2500 scans with a resolution of 2 cm^{-1} . The laser power at the sample was 500 mW.

3. Method of analysis

All the computations in the present study were performed using GAUSSIAN 03 software package [14] and NBO 5.0 [15] programs. The geometry optimization and vibrational frequencies are performed at the B3LYP level using 6-311G* basis set.

Raman activities were computed by numerical differentiation of dipole derivatives with respect to the electric field, using standard GAUSSIAN 03 procedures (Freq = Raman) and default options.

Vibrational assignments are based on comparison of calculated and observed Raman and IR frequencies and activities. The proposed assignments are further corroborated by noting the deuterium isotopic shifts of different bands and their predicted shifts by the same theoretical methods. The assignment of the calculated wavenumbers is aided by the animation option of the GaussView 3.0 graphical interface for Gaussian programs [14,16], which gives a visual representation of the shape of the vibrational modes.

4. Results and discussion

4.1. Molecular geometry

According to the theoretical DFT calculations, two configurations are possible for $\text{Ni}(\text{APO})_2$. These are recognized as trans and cis configurations and are shown in Fig. 1. The optimized geometrical parameters of trans $\text{Ni}(\text{APO})_2$ are summarized in Table 1. The theoretical calculations in the gas phase indicate that the trans configuration is considerably more stable than the cis configuration (about 27.45 kJ mol^{-1}), which is not in agreement with the X-ray result of Gurr [11]. According to the X-ray crystallography, the cis configuration is prominent. This is most likely due to the neglect of solvent effects in our theoretical calculations, which is certainly important (but not easily incorporated) for $\text{Ni}(\text{APO})_2$ complex systems [17,18]. However, Bradbury et al. [19] have shown that $\text{Ni}(\text{APO})_2$ is predominantly trans in solution with the cis and trans isomers in rapid equilibrium at room temperature, therefore both vibrational frequencies and molecular geometry is dependent on the chemical environment. This isomerization probably occurs by twisting to produce a pseudo-tetrahedral intermediate of the type discussed by Holm and O'Connor [20]. Calculations in solution phase show that the energy difference between the cis and trans isomers decreases considerably (about

Table 1

Selected experimental (X-ray) and calculated geometrical parameters for Bis-(4-amino-3-penten-2-ono)nickel(II) (bond lengths in Å, bond angles in °).

Parameter	Ni(APO) ₂		X-ray	Ni(acac) ₂ ^a	APO ^b
	Cis	Trans			
Bond lengths					
Ni–O	1.865	1.853	1.845	1.876	
Ni–N	1.859	1.857	1.843		
O–C	1.274	1.287	1.337	1.273	1.238
N–C	1.318	1.306	1.299		1.348
C9–C10	1.406	1.420	1.405	1.401	1.445
C7–C10	1.395	1.385	1.342		1.375
C6–C14	1.511	1.510	1.475	1.504	1.522
C8–C16	1.513	1.512	1.536		1.505
N–H	1.014	1.014	0.796		1.005
C14–H	1.091	1.091	0.960		
C11–H13	1.081	1.083	0.961		1.083
Bond angles					
O2–Ni–O3	84.66	179.58	85.30	93.6	
O2–Ni–N5	176.8	93.37	178.0		
O2–Ni–N4	92.17	86.63	94.33		
N4–Ni–N5	90.99	179.83	86.11		
O2–C6–C11	124.99	125.56	123.87		123.5
O2–C6–C14	114.71	114.03	116.05		119.5
N4–C8–C11	122.83	121.83	123.76		122.4
N4–C8–C16	118.45	120.07	116.97		116.0
C16–C8–C11	120.30	120.41	120.03		121.6
C6–C11–C8	122.33	123.01	124.37		123.1
Ni–N–H	118.52	114.86	121.45		
C–N–H	112.62	116.12	111.39		
C8–C11–H13	118.62	118.77	118.20		118.2
H4–N4–Ni–N5	0.72		2.74		
O2–Ni–N5–H5		0.5			
H17–C17–C9–N5	158.022	2.752	129.43		
H–C14–C6–O2	179.020	179.729	156.37		
^c ΔE _{gas}	27.45				
ΔE _{solution}	13.07				

^a Data from [21].

^b Calculated at B3LYP/6-311G*.

^c $\Delta E = E_{\text{cis}} - E_{\text{trans}}$ in kJ mol^{-1} .

14.4 kJ mol^{-1}), compared to that in the gas phase. Unfortunately there is no way to predict the energy difference in the solid state. However, this large energy shift may be consistent with the lower energy of the cis form in the solid state.

As it is shown in Table 2, the calculated bond lengths of C–O and C₇–C₁₀ are longer and C–N and C₉–C₁₀ are shorter than the corresponding values in APO. This results show that the resonance in $\text{Ni}(\text{APO})_2$ has increased relative to APO. The calculated Ni–O distance in $\text{Ni}(\text{APO})_2$ is 1.882 Å that is shorter and, therefore, stronger than the similar bond in bis (acetylacetonato) nickel(II) ($\text{Ni}(\text{acac})_2$) [21].

As Table 1 shows, the geometrical parameters are close to the previously determined structural X-ray parameters [11]. The

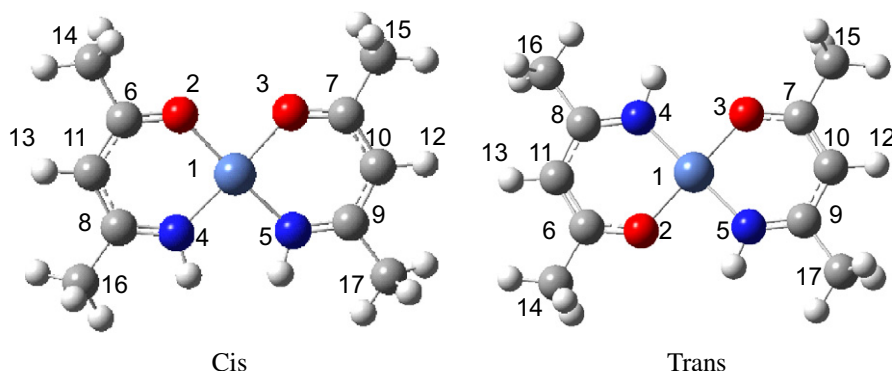


Fig. 1. Cis and Trans configurations and atom numbering of $\text{Ni}(\text{APO})_2$.

Table 2

Selected Wiberg bond orders for Trans and Cis Ni(APO)₂ calculated at B3LYP/6-311G* level of theory.

Bond	Trans	Cis	APO
Ni–O	0.3284	0.3013	1.6169
Ni–N	0.3779	0.4034	1.2810
O–C	1.2785	1.3122	1.1846
N–C	1.5507	1.3121	1.5159
C ₇ –C ₁₀	1.4524	1.4213	1.0040
C ₉ –C ₁₀	1.2479	1.2746	1.0336
C ₇ –C ₁₅	1.0183	1.0177	0.9284
C ₈ –C ₁₆	1.0225	1.0231	1.6169
C ₁₀ –H	0.9241	0.9242	1.2810

Table 3

Selected Natural and Mulliken charges (e) for optimized cis and trans Ni(APO)₂ and APO.

	Natural charges			Mulliken charges	
	Trans	Cis	APO	Trans	Cis
Ni	1.12024	1.12693		1.025550	1.033365
O	-0.73248	-0.69471	-0.64784	-0.560052	-0.513777
N	-0.76367	-0.78843	-0.74366	-0.798333	-0.809356
C6	0.49235	0.50791	0.53593	0.384594	0.376900
C8	0.31202	0.31084	0.30206	0.422570	0.414127
C10	-0.45672	-0.45919	-0.44913	-0.438046	-0.449172
H12	0.19974	0.20014	0.19792	0.182754	0.185978
C14	-0.60833	-0.61366	-0.63875	-0.664854	-0.660902
C16	-0.5993	-0.60002	-0.59718	-0.695745	-0.697576

N–H and C–H_x bond lengths are longer than the corresponding values obtained by X-ray. X-ray diffraction cannot measure the bond lengths including H atom and an electronegative element, such as O or N, exactly. Therefore, the length of such bonds measured by X-ray spectroscopy is shorter than the actual bond length.

The dihedral angle H–C₁₇–C₉–N₅ has deviated from planar structure, by about 22°. However, in X-ray structure, this angle is 129.4, which shows about 50° deviation from planar. This result is also consistent with the crystal effects on the structure of the molecules.

4.2. NBO analysis

The calculated Wiberg bond orders for APO, and cis and trans Ni(APO)₂ are collected in Table 2. This data shows that in both cis and trans Ni(APO)₂ the O–C bond order is significantly less than

and the N–C bond order is considerably greater than the corresponding bond orders in APO. These results confirm that resonance in chelated ring of Ni(APO)₂ is more than in that of APO. Comparison between cis and trans isomers represents that O–C, Ni–N, and C₉–C₁₀ bond orders in the trans isomer are less than and N–C, Ni–O, and C₇–C₁₀ bond orders are greater than cis isomer. The high value of LP(2)O₄ → σ* (Ni–O₂) (305.1 kJ mol⁻¹) and LP(2)C₁₁ → σ* (O₂–C₆) (196.07 kcal mol⁻¹) energies, in the trans isomer and LP(2)O₂ → σ* (Ni–N₅) (66.94 kcal mol⁻¹) and LP(2)C₁₁ → σ* (N₄–C₈) (kJ mol⁻¹) energies, in the cis isomer indicates that these interactions play an important role in the mentioned bond orders.

The charge distribution calculated by the NBO method and the Mulliken charges for optimized geometries of APO, and cis and trans isomers of Ni(APO)₂ are tabulated in Table 3. As this data indicates, the less charge difference over O and N atoms in trans isomer is caused by higher conjugation of Ni–O and Ni–N with C–O and C–N in the trans isomer compared with that in the cis isomer.

4.3. Vibrational analysis

The infrared spectra of Ni(APO)₂ in the solid phase and CH₂Cl₂ solution are shown in Figs. 2 and 3. The far infrared spectrum of the titled compound in the solid phase is shown in Fig. 4. Fig. 5 represents the Raman spectrum of Ni(APO)₂. The theoretical and experimental IR and Raman band frequencies in the solid phase and CHCl₃ and CH₂Cl₂ solutions for cis and trans configurations and their assignments are given in Table 4. Table 5 shows the theoretical and experimental IR band frequencies in the solid phase for Ni(DAPO)₂ along with their assignments. Figs. 6 and 7 show the comparison between the infrared spectra of Ni(APO)₂ and Ni(DAPO)₂ in the solid phase.

The calculated fundamental wavenumbers are compared with the experimental results in the 3400–150 cm⁻¹ region. The calculated frequencies are slightly higher than the observed values for the majority of the normal modes. Two factors may be responsible for the discrepancies between the experimental and computed spectra of Ni(APO)₂. The first is caused by the environment. DFT calculations have been done at the gas phase, and experimental data are obtained from solid complex. The second reason for this discrepancy is the fact that the experimental values are anharmonic frequencies while the calculated values are harmonic frequencies. However, simple scaling of the theoretical wavenumbers according to the equation $\nu_{\text{obsd}} = \alpha \nu_{\text{theor}}$ generally leads to satisfactory agreement with the set of the observed wavenumbers. Values of α for high and low frequencies are used from Ref. [22].

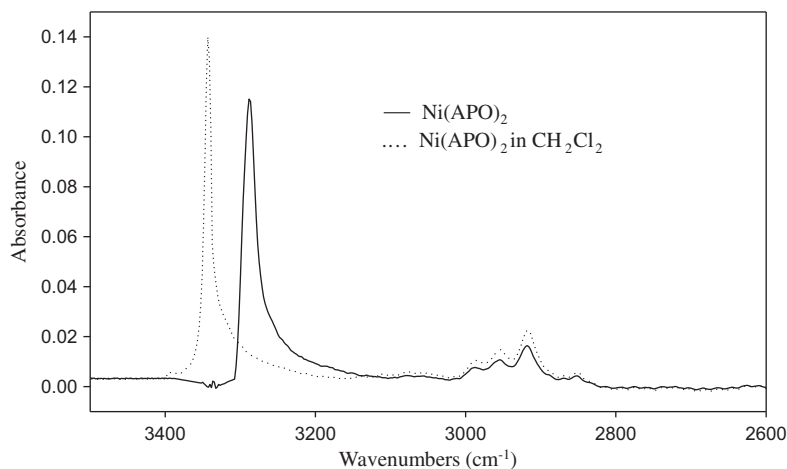


Fig. 2. Infrared spectrum of Ni(APO)₂, in the solid phase and in solution, in the 3500–2600 cm⁻¹ region.

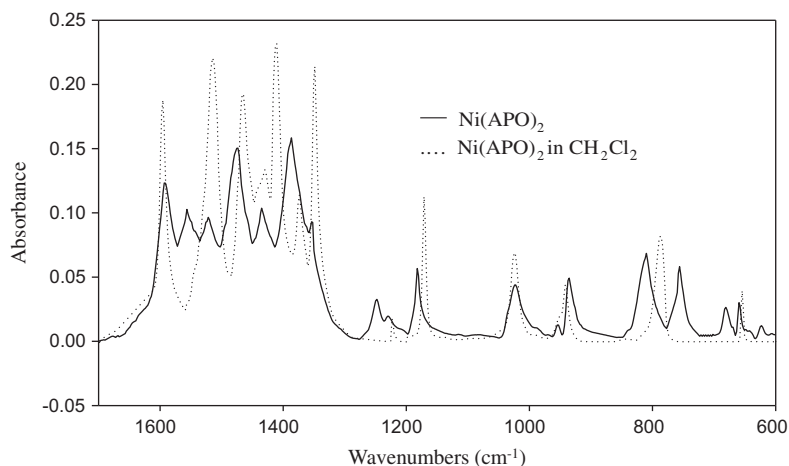


Fig. 3. Infrared spectrum of Ni(APO)₂, in the solid phase and in solution, in the 1700–600 cm⁻¹ region.

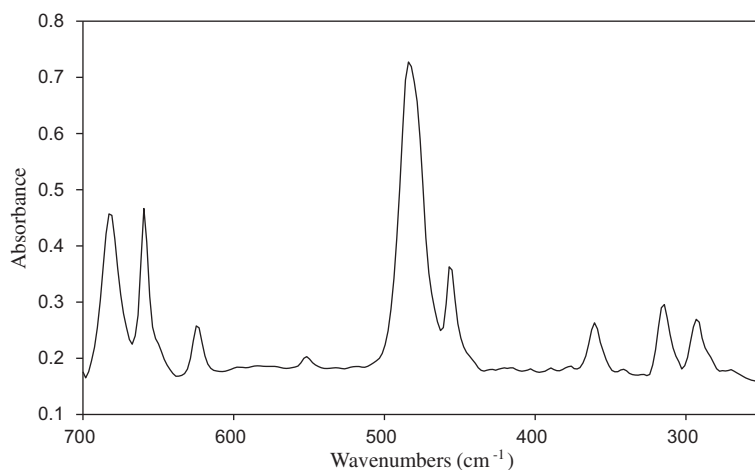


Fig. 4. Far infrared spectrum of Ni(APO)₂, in the solid phase.

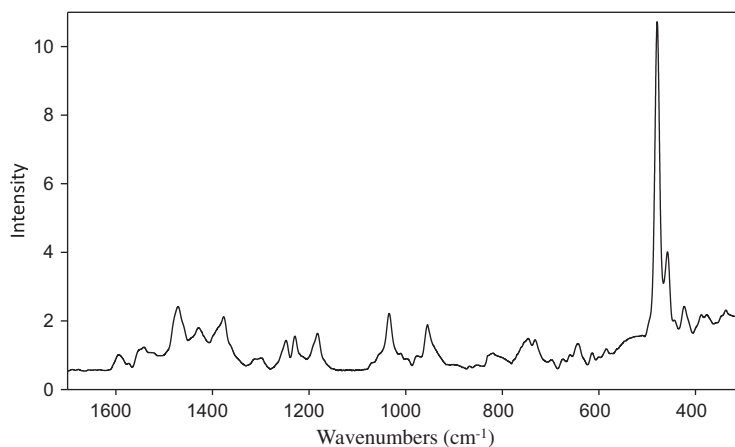


Fig. 5. Raman spectrum of Ni(APO)₂, in the solid phase, in the 1700–250 cm⁻¹ region.

4.3.1. 3500–1700 cm⁻¹ region

In this region the C–H and NH stretching frequencies are expected to be observed. The NH stretching bands are usually appeared in the 3500–3100 cm⁻¹ region upon complexation [23,24]. In the infrared spectrum of Ni(APO)₂ in the solid phase a

strong band is observed at 3287 cm⁻¹. However, in CHCl₃ and CH₂Cl₂ this band shifts to 3346 and 3343 cm⁻¹, respectively. The corresponding band in the deuterated analog appears at 2431 cm⁻¹. The red shift of about 50 cm⁻¹ for this band in the solution, with respect to the solid phase, confirms the presence of a

Table 4
Fundamental band assignment of Ni(APO)₂.

No.	Theoretical				Experimental				Assignment
	Gas		Solution		IR			Raman	
	FsT(I _{IR} , A _R)	FsC(I _{IR} , A _R)	FsT(I _{IR})	FsC(I _{IR})	Solid	CHCl ₃	CH ₂ Cl ₂	Solid	
1	3405(33,1)	3385(4,6)	3402(48)	3393(8)	3287(s)	3346(s)	3343(s)	3288(w)	vN—H
2	3405(0,126)	3379(0,143)	3402(9)	3392(6)				3288	vN—H
3	3068(1,220)	3075(1,227)	3070(2)	3072(6)	3079(w)	(*)	(*)	3082(w)	vCH ₂
4	3068(34,5)	3074(35,3)	3070(45)	3072(41)				3082	vCH ₂
5	2999(44,21)	3000(2143)	3002(0)	3001(29)	2994(w)	3001(w)	2996(w)		vaCH ₃
6	2999(7,134)	3000(49,8)	3002(74)	3001(47)		2985(w)	2981(w)		vaCH ₃
7	2989(46,4)	2998(6,122)	2995(53)	2996(35)	2988(w)				vaCH ₃
8	2989(1,138)	2997(32,39)	2995(23)	2995(35)					vaCH ₃
9	2970(29,1)	2973(30,181)	2972(21)	2975(26)	2956(w)	2964(w)	2962(w)		vaCH ₃
10	2970(0,206)	2973(1,4)	2972(17)	2975(21)		2957(w)			vaCH ₃
11	2966(36,0)	2964(41,148))	2963(54)	2965(34)	2927(w)	2925(w)	2927(vw)		vaCH ₃
12	2966(0,193)	2963(1,29)	2963(2)	2965(21)					vaCH ₃
13	2917(0,625)	2919(29,431)	2920(0)	2919(21)				2917(s)	vsCH ₃
14	2916(35,0)	2919(10,11)	2919(42)	2919(17)	2920(m)	2919(w)	2922(w)	2908(m)	vsCH ₃
15	2916(0,234)	2912(38,366)	2915(0)	2915(65)				2908	vsCH ₃
16	2916(51,2)	2912(7,29)	2915(74)	2915(8)				2908	vsCH ₃
17	1619(0,47)	1599(0,40)	1606(0)	1593(39)				1597(w)	vsC—O, vsC—N(i. p.), δCH ₂
18	1612(381,0)	1586(526,130)	1602(607)	1582(680)	1591(s)	1597(s)	1597(s)		vaC—O, vaC—N(o. p.), δCH ₂
19	1531(0,25)	1562(305,0)	1519(0)	1553(350)				1542(w)	vaC—C—C, δCH ₂ , δNH
20	1528(530,0)	1546(11,5)	1516(753)	1529(110)	1552(s)	1516(m)	1515(w)		vaC—C—C, δCH ₂ , δNH
21	1504(173,0)	1496(308,5)	1486(352)	1483(587)	1523 (s)	1513(s)	1515 (s)		δCH ₃ , vaC—C—N, vaC—C—O
22	1495(0,16)	1488(3,16)	1483(0)	1479(9)				1483(w)	δCH ₃ , vaC—C—N, vaC—C—O
23	1470(0,36)	1478(17,13)	1459(1)	1469(94)	1485(s)			1470(s)	δaCH ₃
24	1469(150,1)	1478(0,12)	1458(320)	1465(78)	1476 (s)	1469(m)	1467(w))		δaCH ₃
25	1461(10,1)	1466(4,22)	1449(17)	1451(52)					δaCH ₃
26	1461(7,26)	1462(166,2)	1449(11)	1447(26)		1466(m)		1462(m)	δaCH ₃
27	1458(0,25)	1456(15,8)	1447(27)	1447(36)		1460(m)	1455(w)	1460(m)	δaCH ₃
28	1458(22,0)	1456(0,19)	1447(6)	1446(188)	1458(m)			1454(w)	δaCH ₃
29	1448(260,0)	1443(378,29)	1427(621)	1438(150)	1434(s)	1436(s)	1442(m)		δaCH ₃ , vaC=C—N, vaC—C=O
30	1437(0,41)	1436(12,21)	1421(0)	1418(76)				1441(w)	δaCH ₃ , vaC=C—N, vaC—C=O
31	1398(0,33)	1433(32,6)	1394(0)	1416(631)	1392(sh)			1401(m)	γCH ₃ , vsC—C=C
32	1391(30,0)	1398(39,5)	1387(46)	1403(94)	1388(vs)	1391(m)	1411(s)		δsCH ₃ , vC—CH ₃
33	1388(0,24)	1389(7,21)	1384(0)	1386(2)				1391(w)	δsCH ₃
34	1385(11,0)	1388(0,0)	1379(14)	1386(0)	1377(sh)	1374(m)	1375(m)	1383(m)	δCH ₃ , vC—CH ₃
35	1380(0,7)	1382(19,17)	1376(0)	1376(5)				1377(s)	δNH, δCH ₂ , δsCH ₃
36	1368(142,0)	1380(5,0)	1366(273)	1375(7)	1352(m)	1350(vs)	1350(s)		δNH, δCH ₂ , δO=C—C
37	1234(7,0)	1247(7,18)	1230(19)	1244(2)	1248(w)	(*)	1225(w)		δNH, δCH ₂ , vC=C—C(i.p.)
38	1219(0,23)	1233(4,8)	1216(0)	1230(12)				1227(m)	δNH, δCH ₂ , vC=C—C(o.p.)
39	1179(61,0)	1198(11,11)	1177(109)	1196(28)	1185(m)	1172(m)	1172(m)		δCH ₂ , δNH
40	1174(0,23)	1186(13,6)	1174(0)	1184(31)				1182(m)	δCH ₂ , δNH
41	1041(0,0)	1042(4,4)	1039(0)	1038(2)					πCH ₃
42	1041(0,0)	1042(0,0)	1028(0)	1037(2)					πCH ₃
43	1035(0,26)	1037(1,19)	1033(0)	1035(6)				1034(m)	ρCH ₃ , δC=C=C
44	1032(27,1)	1033(24,0)	1029(27)	1031(23)	1032(m)	1025(m)	1024(m)		πCH ₃
45	1031(3,0)	1031(27,3)	1029(48)	1028(33)					πCH ₃
46	1031(14,0)	1030(0,0)	1028(1)	1027(6)	1032(m)				ρCH ₃ , δC=C=C
47	1026(0,6)	1026(15,1)	1026(34)	1026(44)					ρCH ₃
48	1026(16,0)	1024(1,0)	1026(0)	1024(13)	1023(m)				ρCH ₃
49	953(0,21)	958(1,25)	951(0)	955(6)				954(s)	δC=C=C, ρCH ₃
50	953(4,0)	957(1,0)	951(11)	953(6)	953(w)				δC=C=C, ρCH ₃
51	933(26,0)	935(12,0)	930(62)	931(45)	935(m)	943(m)	941(m)		Δring, vC—CH ₃
52	925(0,2)	928(0,2)	923(0)	924(4)					Δring, vC—CH ₃
53	780(137,0)	753(96,0)	767(227)	752(165)	814 (vsbr)	(*)	(*)		γCH ₂ , γNH
54	776(0,3)	745(0,0)	764(0)	747(1)				810 (w)	γCH ₂ , γNH
55	737(3,0)	722(7,16)	736(0)	729(12)	767 (vw)			766(w)	γCH ₂ , γNH
56	735(0,1)	698(12,2)	735(0)	710(32)	756 (m)				γCH ₂ , γNH
57	733(9,0)	691(2,0)	729(18)	696(1)		(*)	(*)		vaN—Ni—N, δC=C—N
58	704(0,17)	675(16,3)	703(0)	678(0)				704(w)	vsN—Ni—N, vsO—Ni—O(i.p.)
59	681(21,0)	662(0,0)	677(37)	669(34)	681(m)	(*)	(*)		vaO—Ni—O
60	640(38,0)	637(69,0)	635(77)	635(105)	659(m)		651(m)		Γring
61	626(0,1)	612(7,0)	624(0)	607(10)					Γ
62	625(0,5)	559(0,2)	622(0)	602(0)	623(vw)				vsO—Ni—O, vsN—Ni—N(o.p.)
63	531(0,0)	531(0,4)	532(0)	534(0)					γC—CH ₃
64	524(0,4)	530(0,1)	526(0)	532(0)					γC—CH ₃
65	489(37,0)	477(41,0)	483(64)	470(71)	485(vs)	492(s)	487(s)		vaO—Ni—O, vaN—Ni—N
66	468(0,22)	470(0,14)	465(0)	469(1)				479(vs)	vsO—Ni—O, vsN—Ni—N
67	451(2,0)	450(4,8)	449(4)	446(7)	456(s)				δaC—CH ₃
68	410(0,3)	420(0,1)	409(0)	416(0)					δaC—CH ₃
69	376(2,0)	369(1,0)	374(2)	370(1)					vaN—Ni—N, δO—Ni—O
70	361(6,0)	357(6,0)	358(10)	351(8)	361(m)				δN—Ni—N, δO—Ni—O
71	327(6,0)	324(7,0)	316(13)	316(15)	315(w)				γN—Ni—N, γO—Ni—O

(continued on next page)

Table 4 (continued)

Theoretical				Experimental				Assignment
Gas			Solution	IR			Raman	
No.	FsT(I _{IR} , A _R)	FsC(I _{IR} , A _R)	FsT(I _{IR})	FsC(I _{IR})	Solid	CHCl ₃	CH ₂ Cl ₂	Solid
72	285(0,3)	282(1,2)	285(0)	283(2)				278(s)
73	267(0,6)	270(0,3)	265(0)	273(1)				265(s)
74	262(1,0)	253(1,5)	262(2)	248(3)				
75	215(0,5)	214(0,4)	213(0)	214(0)				
76	209(3,0)	196(0,0)	199(6)	196(0)	196(s)			
77	169(0,2)	157(6,1)	157(0)	156(1)				
78	164(3,0)	157(0,0)	159(4)	155(9)				
79	148(0,1)	143(0,0)	136(0)	137(0)				
80	129(0,3)	111(1,0)	118(0)	112(2)				
81	113(5,0)	105(0,3)	111(8)	107(0)				
82	110(0,1)	92(4,0)	105(6)	102(8)				
83	107(3,0)	75(0,2)	97(0)	63(0)				
84	52(0,0)	49(1,3)	48(0)	41(1)				
85	46(1,0)	46(0,0)	39(6)	37(0)				
86	35(0,0)	38(1,0)	37(0)	31(1)				
87	34(2,0)	25(0,0)	37(0)	28(1)				

^a Fs., theoretical frequency calculated at the UB3LYP/6-311G* level, scaled by 0.9600 and 0.9781 for the 2000–3600 cm⁻¹ and below 1700 cm⁻¹ regions, respectively.); C, Cis; T, Trans; I_{IR}, IR intensity (in km/mol); and A_R, Raman activity (Å⁴/amu), the relative intensities are given in parentheses; v, very; s, strong; m, medium; w, weak; sh, shoulder; (*), solvent band overlap, v, stretching; δ, in-plane bending; γ, out-of-plane bending; Δ, in-plane ring deformation; Γ, out-of-plane ring deformation; τ, torsion; ρ, in-plane rocking; π, out-of-plane rocking; i.p, in phase; o.p. out of phase.

weak intermolecular hydrogen bond in the solid phase. Archer [25] reported a band at 3285 cm⁻¹ without any band assignment. The corresponding band in Cu(APO)₂ in the solid phase is observed at 3290 cm⁻¹ [26]. The infrared band at 3079 cm⁻¹ and Raman band at 3082 cm⁻¹ are assigned to the CH₂ stretching and a series of weak bands, which are observed in the 2994–2920 cm⁻¹ range, are assigned to the asymmetric and symmetric CH₃ stretching. These bands did not change significantly upon deuteration.

4.3.2. 1700–1000 cm⁻¹ region

This is the most significant region of spectra. Beside the CH₃ and NH deformation and rocking frequencies, C–CH₃ stretching, and CH in-plane bending modes, four bands are expected to be observed in this region per ligand in relation to the chelated ring modes which are attributed to the C–O, C–C, C=C, and C–N stretching movements. Since there are two ligands per molecule, it is expected that these vibrational modes to be appeared as in-phase and out-of-phase vibrational modes. The infrared spectrum of Ni(APO)₂ in the solid phase showed a strong band at 1591 cm⁻¹.

According to the theoretical calculations, this band is assigned to the out-of-phase C–O and C–N stretching. The corresponding in-phase band in the Raman spectrum was observed at 1597 cm⁻¹. Two strong infrared bands observed at 1485 and 1552 cm⁻¹ in the solid phase. The former is due to the in-plane bending of CH₃ and the latter is assigned to the asymmetric C–C=C stretching which is coupled with the CH₂ and NH in-plane bending modes. The latter shifts to about 1515 cm⁻¹ in the CHCl₃ and CH₂Cl₂ solutions. Upon deuteration, the 1552 cm⁻¹ band shifts to 1514 cm⁻¹. This result suggests that the intermolecular hydrogen bond disappears in solution. Disappearing of this band in the IR spectrum of deuterated compound supports this assignment.

The strong infrared band at 1523 cm⁻¹ is attributed to the CH₃ deformation coupled with the asymmetric C–C–O and C–C–N stretching modes. This band shifts to about 1515 cm⁻¹ in the CHCl₃ and CH₂Cl₂ solutions. Upon deuteration, this band shifts to 1514 cm⁻¹. The strong infrared band at 1434 cm⁻¹ is also associated to the asymmetric CH₃ bending which is coupled with the asymmetric C=C–N and C–C=O stretching. The corresponding band in Cu(APO)₂ was observed at 1435 cm⁻¹ [26]. The very strong infrared band at 1388 cm⁻¹ is attributed to symmetric CH₃ bending. The 1185 cm⁻¹ band is assigned to the CH₂ in-plane bending mode

which is somewhat coupled to the N–H in-plane bending. The corresponding band in Cu(APO)₂ [26], acetylacetonate, AA, [27], magnesium acetylacetonate, Mg(acac)₂, [21], and beryllium acetylacetonate, Be(acac)₂, [28] is observed at 1180, 1173, 1198, and 1191 cm⁻¹, respectively.

4.3.3. Below 1000 cm⁻¹

In this region, one expects to observe C–CH₃ stretching, N–H, and C–H out-of-plane bending, in-plane, and out-of-plane ring deformations. Archer [25] reported eight bands in this region: 950, 935, 810, 790, 755, 710, 680, and 650 cm⁻¹. The strong Raman band at 954 cm⁻¹ is assigned to the C–C=C bending which is coupled with the CH₃ rocking. The infrared band at 935 cm⁻¹ in the solid phase is related to the in-plane ring deformation which is coupled with C–CH₃ stretching. The solid state infrared broad bands at 814 and 767 cm⁻¹ are assigned to the CH₂ and NH out-of-plane bending modes. Upon deuteration, these bands move to 757 and 538 cm⁻¹. According to the theoretical calculations the former is assigned to the CH₂ out-of-plane bending and the latter is related to the ND out-of-plane bending. The infrared bands at 681 and 659 cm⁻¹ are assigned to the asymmetric O–Ni–O stretching and out-of-plane ring deformation, respectively. The very strong infrared and Raman bands at 485 and 479 cm⁻¹ are assigned to the asymmetric and symmetric O–Ni–O stretching (coupled with the N–Ni–N stretching), respectively. The corresponding bands in Cu(APO)₂ were reported to be occurred at 466 and 464 cm⁻¹ [26]. The two infrared bands at 315 and 196 cm⁻¹ are assigned to the O–Ni–O and N–Ni–N out-of-plane bending modes, respectively.

5. Conclusion

According to the theoretical DFT calculations, the trans configuration in the gas phase is more stable than cis (about 27.45 kJ mol⁻¹). But, in solution, the energy difference between the cis and trans isomers decreases about 14.4 kJ mol⁻¹. The calculated bond lengths of C–O, and C₉–C₁₀ (Table 1) are longer and C–N and C=C(O) are shorter than the corresponding ones in APO. These results show that resonance in Ni(APO)₂ is increased compared with APO. The Ni–O distance in Ni(APO)₂ is 1.86 Å,

Table 5
Fundamental band assignment of Ni(DAPO)₂.

No.	Theoretical						Experimental IR _{solid}	Assignment
	Trans			Cis				
	Fs	I _{IR}	A _R	Fs	I _{IR}	A _R		
1	3068	1	221	3075	1	228	3082(w)	νCH ₂
2	3068	34	5	3074	35	3		νCH ₂
3	2999	43	23	3000	2	143	2994(w)	νaCH ₃
4	2999	8	132	3000	49	8	2987(w)	νaCH ₃
5	2989	46	4	2998	6	123		νaCH ₃
6	2989	1	139	2997	32	39	2954(w)	νaCH ₃
7	2970	29	1	2973	30	181		νaCH ₃
8	2970	0	206	2973	1	4		νaCH ₃
9	2966	36	0	2964	40	148		νaCH ₃
10	2966	0	193	2963	1	29	2927(w)	νaCH ₃
11	2917	0	625	2919	29	431		νsCH ₃
12	2916	35	0	2919	10	11	2917(m)	νsCH ₃
13	2916	0	234	2912	38	367		νsCH ₃
14	2916	51	2	2912	7	29		νsCH ₃
15	2493	31	0	2478	6	3	2431(s)	νN–D
16	2493	0	55	2472	1	66		νN–D
17	1616	0	48	1597	0	40		νaC–O, νaC–N(o.p.), δCH ₂
18	1608	376	0	1583	526	0	1587(s)	νaC–O, νaC–N(o.p.), δCH ₂
19	1520	0	32	1534	420	3		νaC–C=C, δCH ₂
20	1519	668	0	1530	46	5	1514(s)	νaC–C=C, δCH ₂
21	1498	81	0	1494	220	4	1496(s)	νaC–C=O, νaC–C=N(o.p.), δaCH ₃ , δCH ₂
22	1494	0	14	1488	2	16		νaC–C=O, νaC–C=N(o.p.), δaCH ₃ , δCH ₂
23	1468	1	42	1477	16	14	1460(m)	δaCH ₃
24	1468	122	1	1477	1	12	1460(m)	δaCH ₃
25	1461	9	2	1463	1	41		δaCH ₃
26	1461	8	26	1461	136	3		δaCH ₃
27	1458	0	24	1456	15	8	1450(m)	δaCH ₃
28	1458	22	0	1456	0	19	1448(m)	δaCH ₃
29	1445	300	0	1442	359	8	1437(s)	δaCH ₃ , νaC=C–N, νaC–C=O
30	1436	0	42	1430	16	8	1430(m)	δaCH ₃ , νaC=C–N, νaC–C=O
31	1391	0	31	1389	4	28		δsCH ₃
32	1391	15	0	1389	1	4	1392(vs)	δsCH ₃
33	1384	11	0	1383	25	20		δsCH ₃
34	1384	0	18	1383	0	2		δsCH ₃
35	1312	0	6	1324	1	16		δC=C–C, νC–CH ₃ , δND, δCH ₂
36	1305	63	0	1316	32	0	1303(s)	δC=C–C, νC–CH ₃ , δND, δCH ₂
37	1215	31	0	1218	18	1	1198(w)	δCH ₂ , νC–CH ₃
38	1209	0	19	1213	8	15		δCH ₂ , νC–CH ₃
39	1041	2	0	1054	3	0		πCH ₃
40	1040	1	0	1046	27	0	1022(m)	πCH ₃ , δND
41	1040	27	0	1042	4	4		ρCH ₃ , δC=C–C, ND
42	1039	0	19	1042	0	0		πCH ₃
43	1031	18	0	1032	4	15		πCH ₃
44	1030	0	0	1030	28	1		ρCH ₃ , δCH ₂
45	1029	18	0	1030	0	0		πCH ₃
46	1028	0	1	1027	10	0		ρCH ₃ , δCH ₂
47	966	18	0	992	5	15	953(w)	δND, ρCH ₃ , δC–C–N, νC–CH ₃ , νaN–Ni–N
48	961	0	7	967	5	0		δND, ρCH ₃ , νC–CH ₃ , δC–C=C, νsN–Ni–N
49	950	0	28	957	2	25	934(w)	δC–C=C, ρCH ₃
50	949	6	0	956	1	0		δND, νC–CH ₃ , δC–C=C, νsN–Ni–N
51	926	34	0	933	13	1	922(w)	Δring, νC–CH ₃
52	920	0	4	926	1	2		Δring, νC–CH ₃
53	747	51	0	743	49	0	757(w)	γCH ₂
54	746	0	0	742	0	0		γCH ₂
55	695	24	0	688	13	13	682(w)	νaO–Ni–O, νaN–Ni–N, δND
56	672	5	0	672	9	8		νsO–Ni–O, νsN–Ni–N, δND
57	670	0	14	664	2	0	664(w)	νaO–Ni–O, νaN–Ni–N, δND, γC–CH ₃
58	653	4	0	656	10	1		Γ
59	648	0	1	649	0	0		Γ
60	607	0	11	592	8	0		νsO–Ni–O, νsN–Ni–N(o.p.)
61	569	75	0	533	0	0	538(w)	γND
62	549	0	2	531	3	4		γND
63	530	1	0	520	68	0		γC–CH ₃
64	524	0	4	475	39	0		γC–CH ₃
65	487	36	0	466	0	15	480(s)	νaO–Ni–O, νaN–Ni–N
66	465	0	22	448	4	7		νsO–Ni–O
67	447	2	0	435	0	3		δaC–CH ₃
68	408	0	3	418	0	1		δaC–CH ₃
69	374	2	0	368	1	0		νsO–Ni–O, νsN–Ni–N
70	360	6	0	356	6	0		δO–Ni–O, δN–Ni–N
71	318	4	0	315	4	0		γO–Ni–O, γN–Ni–N

(continued on next page)

Table 5 (continued)

No.	Theoretical						Experimental IR _{solid}	Assignment
	Trans			Cis				
	Fs	I _{IR}	A _R	Fs	I _{IR}	A _R		
72	284	0	3	281	1	2	δAPO–Ni–APO	
73	267	0	6	269	0	2	δC–CH ₃	
74	262	1	0	253	1	5	δC–CH ₃	
75	214	0	4	213	0	4	Δ	
76	206	3	0	192	0	0	νsN–Ni–N, νsO–Ni–O(o.p.)	
77	168	0	1	156	0	0	δC–CH ₃	
78	163	3	0	155	6	0	νAPO–Ni–APO	
79	146	0	1	143	0	0	τC–N–Ni, γC–CH ₃	
80	128	0	3	110	1	0	τC–O–Ni, γC–CH ₃	
81	113	5	0	104	0	3	τCH ₃	
82	109	0	1	92	4	0	δAPO–Ni–APO	
83	106	3	0	73	0	2	τCH ₃ , τAPO–Ni–APO	
84	51	0	0	49	1	3	τCH ₃ , τAPO–Ni–APO	
85	45	1	0	46	0	0	γAPO–Ni–APO	
86	35	0	0	38	1	0	τCH ₃	
87	34	2	0	25	0	0	τCH ₃	

^a Fs., theoretical frequency calculated at the UB3LYP/6-311G* level, scaled by 0.9600 and 0.9781 for the 2000–3600 cm⁻¹ and below 1700 cm⁻¹ regions, respectively.); I_{IR}, IR intensity (in km/mol); v, very; s, strong; m, medium; w, weak; sh, shoulder; br, broad; (*), solvent band overlap, ν, stretching; δ, in-plane bending; γ, Δ, in-plane ring deformation; Γ, out-of-plane ring deformation; τ, torsion; ρ, in-plane rocking, π, out-of-plane rocking; i.p. in phase; o.p. out of phase.

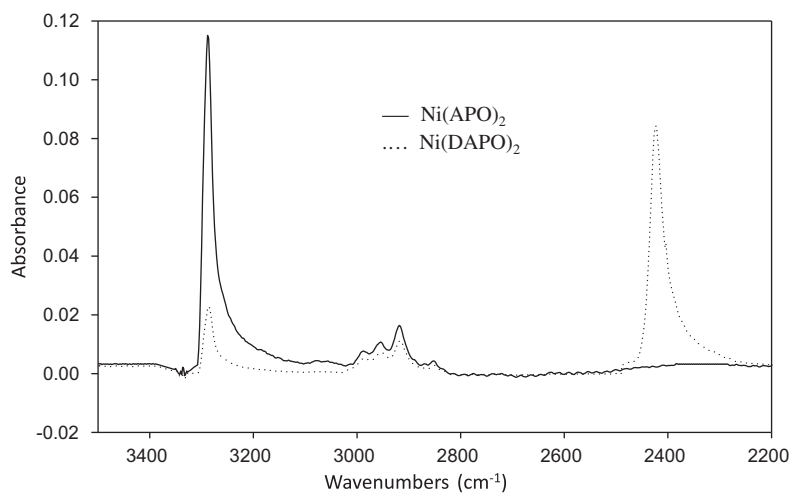


Fig. 6. Comparison between the infrared spectra of Ni(APO)₂ and Ni(DAPO)₂ in the solid phase in the 3500–2200 cm⁻¹ region.

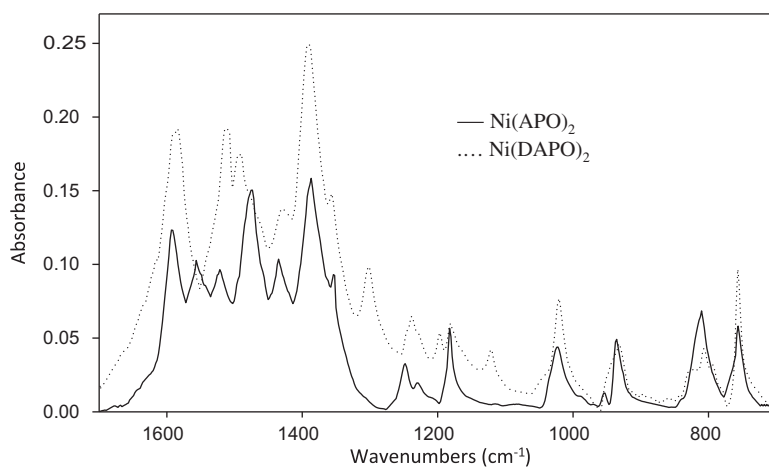


Fig. 7. Comparison between the infrared spectra of Ni(APO)₂ and Ni(DAPO)₂ in the solid phase in the 1700–700 cm⁻¹ region.

which is longer and, therefore, weaker than the corresponding bond in Ni(acac)₂.

The scaled calculated and observed frequencies, except for N–H vibrational band frequencies, are in excellent agreement. The red

shifts in N–H band frequencies are attributed to the formation of intermolecular hydrogen bonding in the solid phase and in solution with polar solvents.

References

- [1] T.V. Laine, K. Lappalainen, J. Liimatta, E. Aitola, B. Lofgren, M. Leskela, *Macromol. Rapid Commun.* 20 (1999) 487.
- [2] G.J.P. Britovsek, V.C. Gibson, S. Mastroianni, D.C.H. Oakes, C. Redshaw, G.A. Solan, A.J.P. White, D.J. Williams, *Eur. J. Inorg. Chem.* 2001 (2001) 431.
- [3] S. Mecking, *Macromol. Rapid Commun.* 20 (1999) 139.
- [4] G.J.P. Britovsek, S. Mastroianni, G.A. Solan, S.P.D. Baugh, C. Redshaw, V.C. Gibson, A.J.P. White, D.J. Williams, M.R.J. Elsegood, *Chem. Eur. J.* 6 (2000) 2221.
- [5] S.D. Ittel, L.K. Johnson, M. Brookhart, *Chem. Rev.* 100 (2000) 1169.
- [6] S. Mecking, *Angew. Chem. Int. Ed.* 40 (2001) 534.
- [7] V.C. Gibson, S.K. Spitzmesser, *Chem. Rev.* 103 (2003) 283.
- [8] L.S. Boffa, B.M. Novak, *Chem. Rev.* 100 (2000) 1479.
- [9] X. He, Q. Wu, *Appl. Organometal. Chem.* 20 (2006) 264.
- [10] X. He, Y. Yao, X. Luo, J. Zhang, Y. Liu, L. Zhang, Q. Wu, *Organometallics* 22 (2003) 4952.
- [11] G.E. Gurr, *Inorg. Chem.* 3 (1964) 614.
- [12] M.J. Lacey, *Aust. J. Chem.* 23 (1970) 841.
- [13] M. Ghaffari, M.Sc Thesese, Ferdowsi University of Mashhad, 2010.
- [14] M.J. Frisch, G.W. Trucks, H.B. Schlegel, G.E. Scuseria, M.A. Robb, J.R. Cheeseman, J.A. Montgomery Jr., T. Vreven, K.N. Kudin, J.C. Burant, J.M. Millam, S.S. Iyengar, J. Tomasi, V. Barone, B. Mennucci, M. Cossi, G. Scalmani, N. Rega, G.A. Petersson, H. Nakatsuji, M. Hada, M. Ehara, K. Toyota, R. Fukuda, J. Hasegawa, M. Ishida, T. Nakajima, Y. Honda, O. Kitao, H. Nakai, M. Klene, X. Li, J.E. Knox, H.P. Hratchian, J.B. Cross, V. Bakken, C. Adamo, J. Jaramillo, R. Gomperts, R.E. Stratmann, O. Yazyev, A.J. Austin, R. Cammi, C. Pomelli, J.W. Ochterski, P.Y. Ayala, K. Orokuma, G.A. Voth, P. Salvador, J.J. Dannenberg, V.G. Zakrzewski, S. Dapprich, A.D. Daniels, M.C. Strain, O. Farkas, D.K. Malick, A.D. Rabuck, K. Raghavachari, J.B. Foresman, J.V. Ortiz, Q. Cui, A.G. Baboul, S. Clifford, J. Cioslowski, B.B. Stefanov, G. Liu, A. Liashenko, P. Piskorz, I. Komaromi, R.L. Martin, D.J. Fox, T. Keith, M.A. Al-Laham, C.Y. Peng, A. Nanayakkara, M. Challacombe, P.M.W. Gill, B. Johnson, W. Chen, M.W. Wong, C. Gonzalez, J.A. Pople, *Gaussian 03, Revision B.03*, Gaussian, Inc., Wallingford, CT, 2004.
- [15] F. Weinhold, C.R. Landis, *Chem. Ed. Res. Pract. Eur.* 2 (2001) 91.
- [16] GaussView 3.0, Gaussian Inc., Carnegie Office Park, Pittsburgh, PA 15106, USA.
- [17] A. Shimizu, T. Mori, Y. Inoue, S. Yamada, *J. Phys. Chem. A* 113 (2009) 8754.
- [18] M. Nishizaka, T. Mori, Y. Inoue, *J. Phys. Chem. Lett.* 1 (2010) 1809.
- [19] J.R. Bradbury, J.L. Hampton, D.P. Martone, A.W. Maverick, *Inorg. Chem.* 28 (1989) 2392.
- [20] R.H. Holm, M.J. O'Connor, *Prog. Inorg. Chem.* 14 (1971) 241.
- [21] S. Shibata, M. Ohta, R. Tani, *J. Mol. Struct.* 73 (1981) 119.
- [22] S.F. Tayyari, T. Bakhshi, S.J. Mahdizadeh, S. Mehrani, R.E. Sammelson, *J. Mol. Struct.* 938 (2009) 76.
- [23] J.W. Davis, J. Smith, *J. Chem. Soc., A* 317 (1971).
- [24] B.J. Hodgson, C.G. Percy, A.D. Thornton, *Spectrochim. Acta* 35A (1979) 949.
- [25] R.D. Archer, *Inorg. Chem.* 2 (1963) 292.
- [26] M. Jamialahmadi, S.F. Tayyari, M.H. Habibi, M. Yazdanbakhsh, S. Kadkhodaei, R.E. Sammelson, *J. Mol. Struct.* 985 (2011) 139.
- [27] S.F. Tayyari, F. Milani-Nejad, *Spectrochim. Acta* 56A (2000) 2679.
- [28] S.F. Tayyari, T. Bakhshi, M. Ebrahimi, R.E. Sammelson, *Spectrochim. Acta* 73A (2009) 342.